Supplementary Information for

Nano-scale Control of the Ionomer Distribution by Molecular Masking of the Pt Surface in PEMFCs

Gisu Doo,[a] Seongmin Yuk,[a] Ji Hye Lee,[c] Sungyu Choi,[a] Dong-Hyun Lee,[a] Dong Wook Lee,[a] Jonghyun Hyun,[a] Sung Hyun Kwon,[c] Seung Geol Lee*[c] and Hee-Tak Kim*[a,b]

[a]Department of Chemical and Biomolecular Engineering, KAIST, Daejeon 34141, Republic of Korea

[b]Advanced Battery Center, KAIST Institute for the NanoCentury, KAIST, Daejeon 34141, Republic of Korea

[c]Department of Organic Material Science and Engineering, Pusan National University, Busan 46241, Republic of Korea

*E-mails: (H.-T. Kim) heetak.kim@kaist.ac.kr; (S. G. Lee)seunggeol.Lee@pusan.ac.kr

Figures

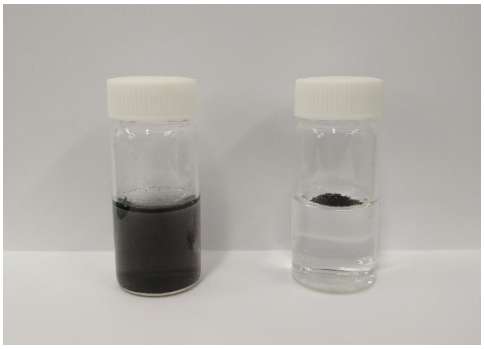

Fig. S1 Water dispersibility of catalyst particles. Optical images of Pt/C (left) and ODT-Pt/C (right) dispersed in water.

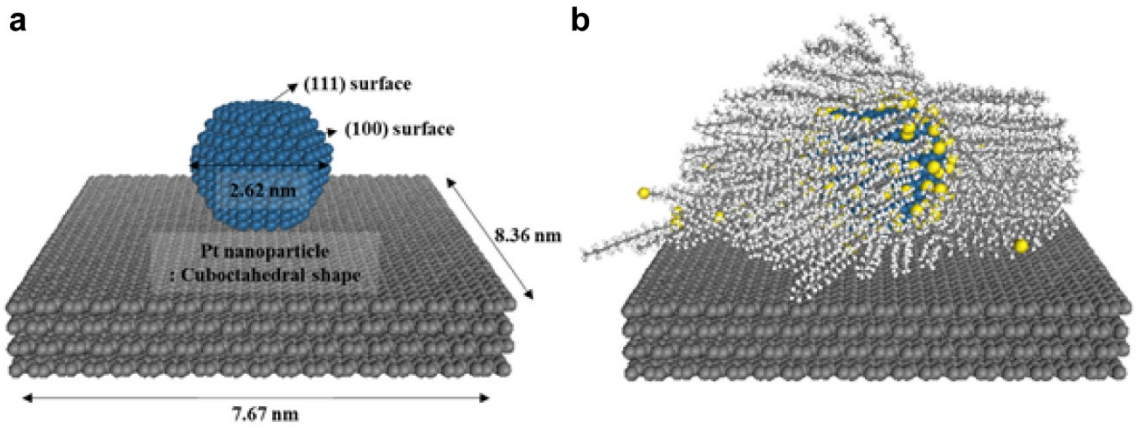

Fig. S2 MD simulations of alkanethiol adsorption on polycrystalline Pt nanoparticle. (a, b) A model for a Pt nanoparticle supported on carbon surface (a) and at the maximum adsorption of the ODT on the Pt surface (b).

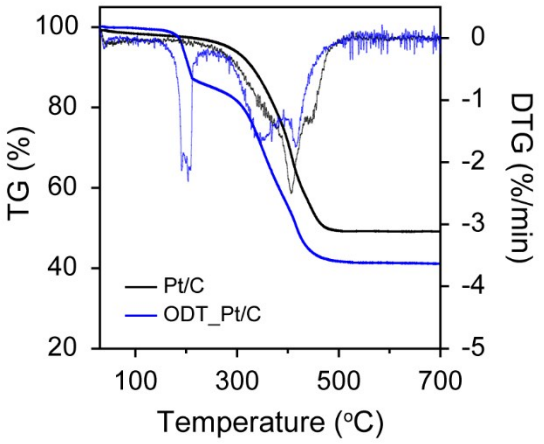

Fig. S3 Thermogravimetric analysis of Pt/C and ODT-Pt/C under air. The scan rate of thermal sweep was set to 5 °C min^{-1}. Pt/C has a weight loss at 300 to 500 °C, which corresponds to the carbon oxidation, whereas the ODT-Pt/C has an additional weight loss at around 200 °C because of the ODT adsorbed on catalyst particles.

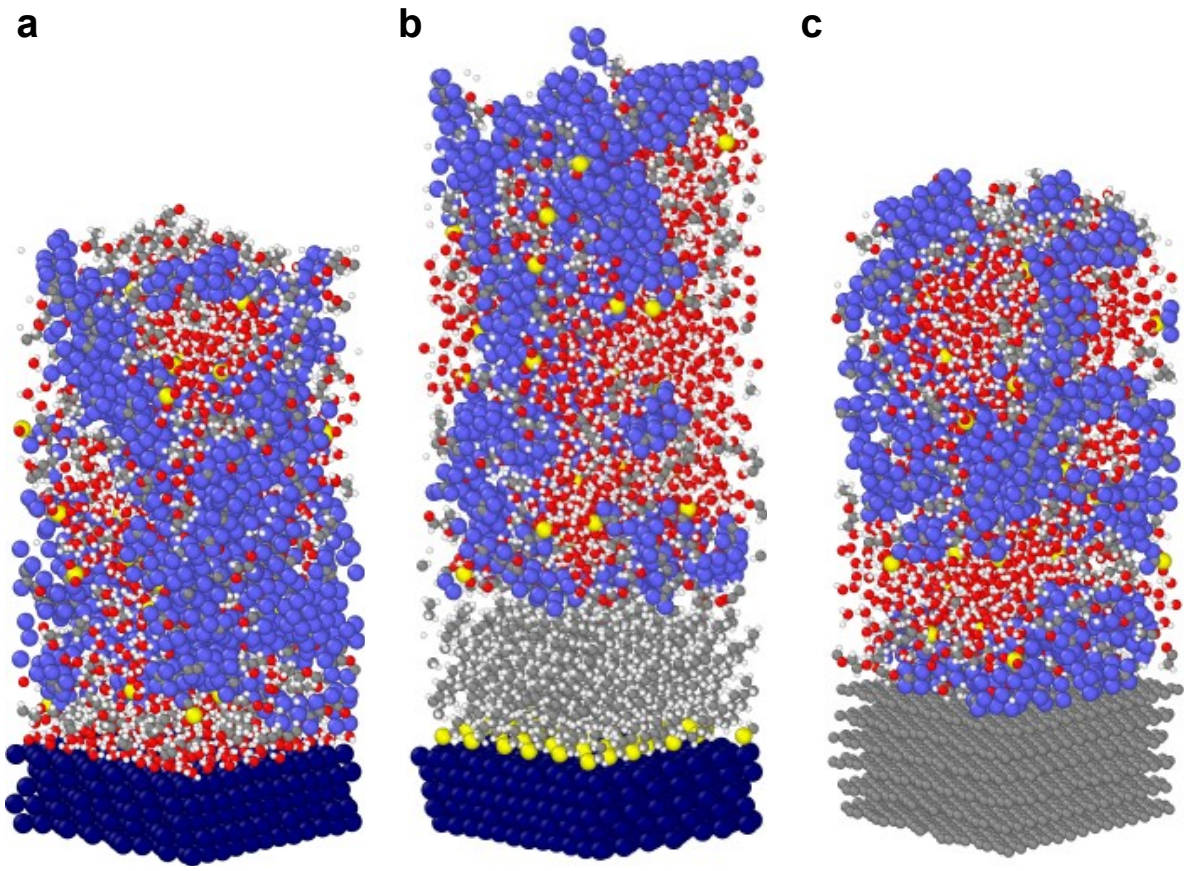

Fig. S4 Equilibrium structures of the Nafion ionomer dispersions. (a-c) Nafion ionomer dispersions on Pt surface (a), ODT-Pt surface (b) and carbon surface (c). The white, gray, red, light blue, yellow and deep blue denote the hydrogen, carbon, oxygen, fluorine, sulfur and platinum atoms, respectively.

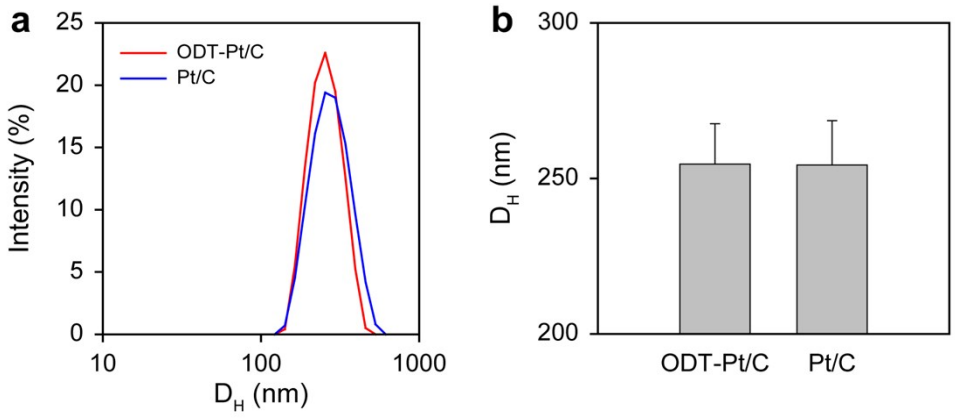

Fig. S5 DLS measurements of the diluted slurries with ODT-Pt/C and the bare Pt/C. (a) The intensity plots of the hydrodynamic diameter (D_H) of the slurries and (b) the averaged values of the D_H.

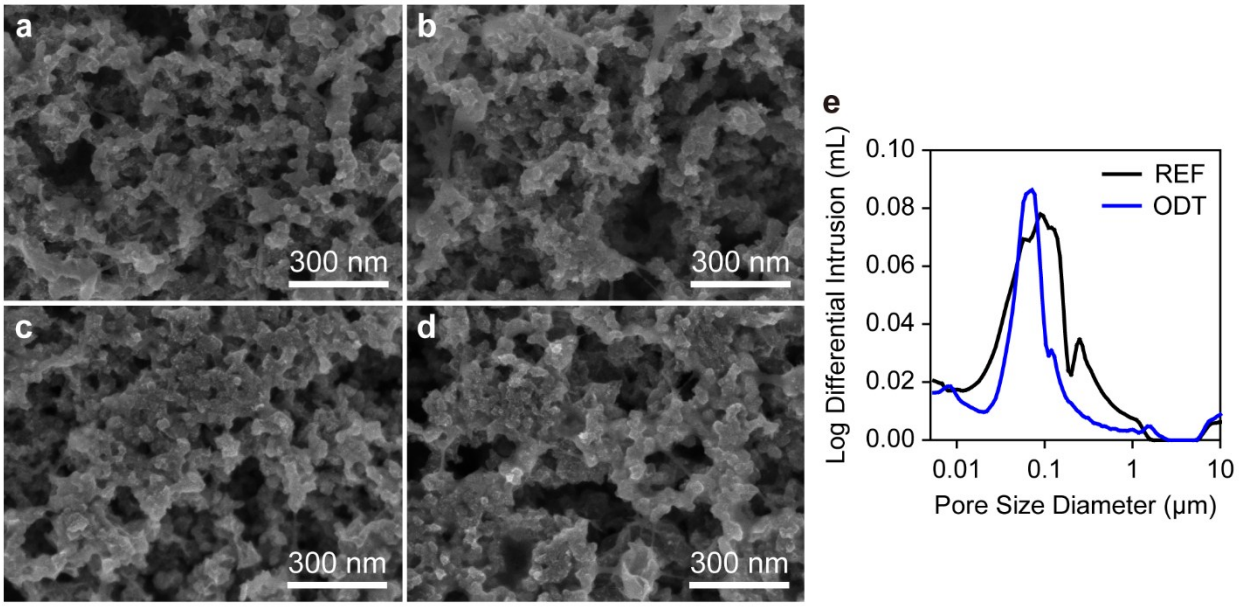

Fig. S6 SEM images and mercury intrusion porosimetry data of CLs. (a, b) CLs with Pt/C and (c, d) CLs with ODT-Pt/C. (e) Comparison of mercury intrusion porosimetry data for CL with Pt/C and that with ODT-Pt/C

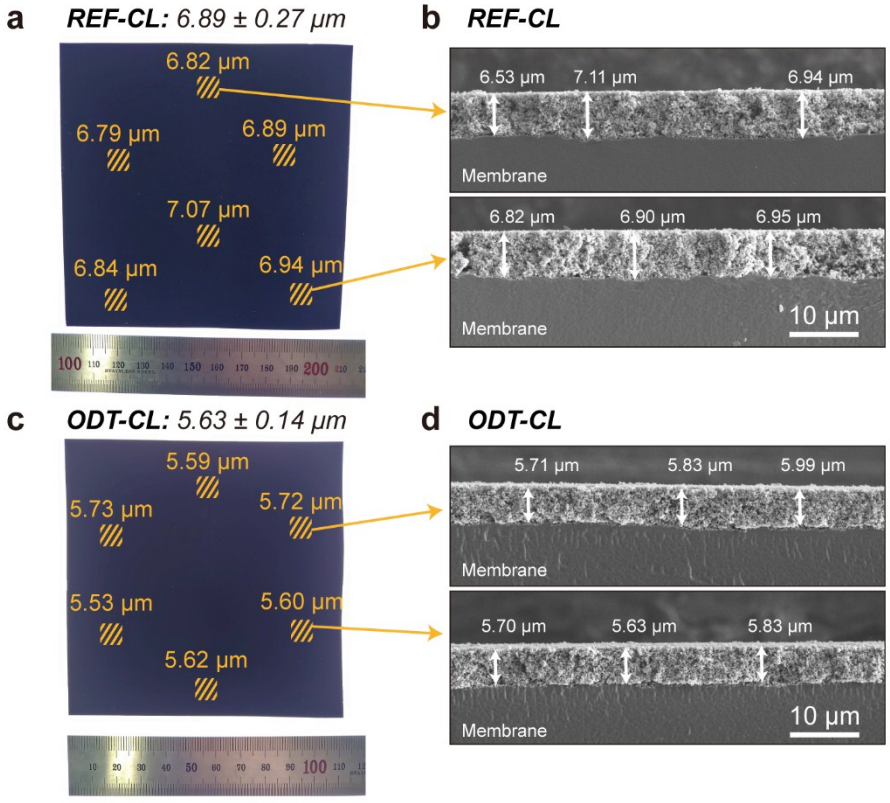

Fig. S7 Optical images of (a) a bare catalyst layer and (b) an ODT treated catalyst layer, and their thickness measured from the cross-sectional SEM images. The average thickness of each orange spot is noted on the optical images, and the total average and standard deviation values are written on the top. (b, d) Examples of the catalyst layer cross-section images with SEM.

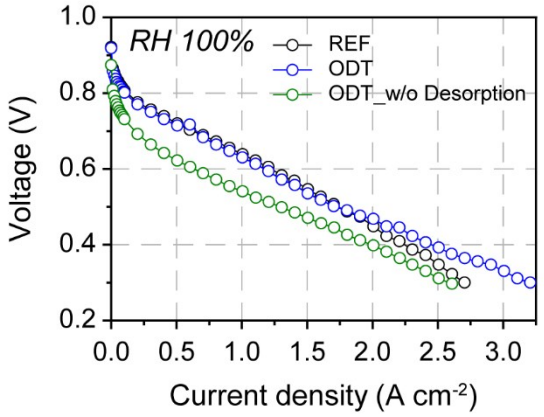

Fig. S8 Comparison of the IV polarization curves with and without the desorption process. All the curves are under H_2/air with RH 100% of gas flow injected.

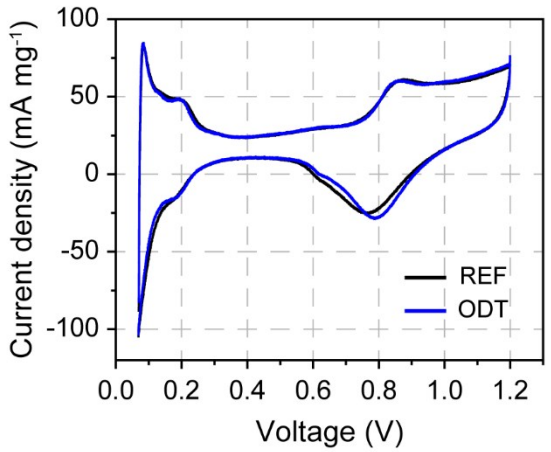

Fig. S9 Cyclic voltammetry (CV) plots for the cells. The CV shows the almost identical ECSA values for the REF and ODT cells. The CV was recorded with hydrogen flow in the anode and nitrogen gas filled cathode without any flows. The scan rate was set to 50 mV s^{-1}.

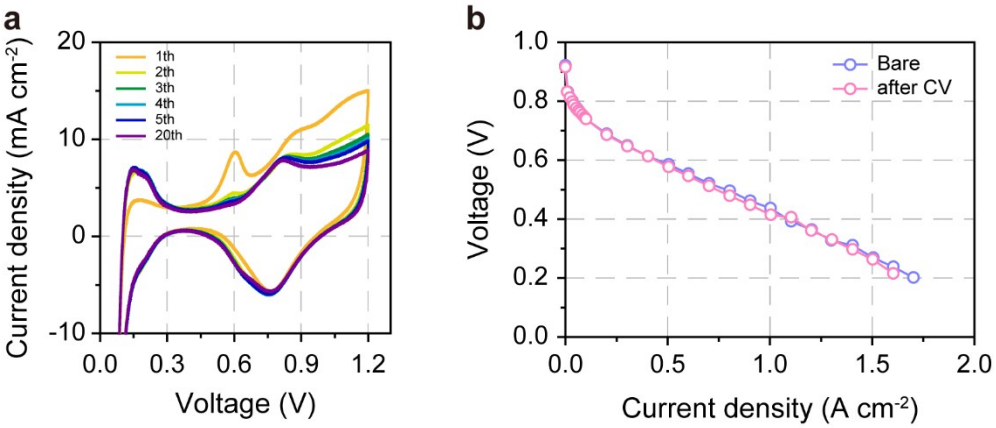

Fig. S10 (a) CV curves of the REF cell during the 20 cycles in the potential range of 0.07 to 1.2 V used in the thiol desorption. The responses reached an equilibrium within 5 cycles, and they did not show any significant differences between 5 and 20 cycles. (b) IV polarization curves of REF cells before and after the CV cycling at RH 50 % without back pressure.

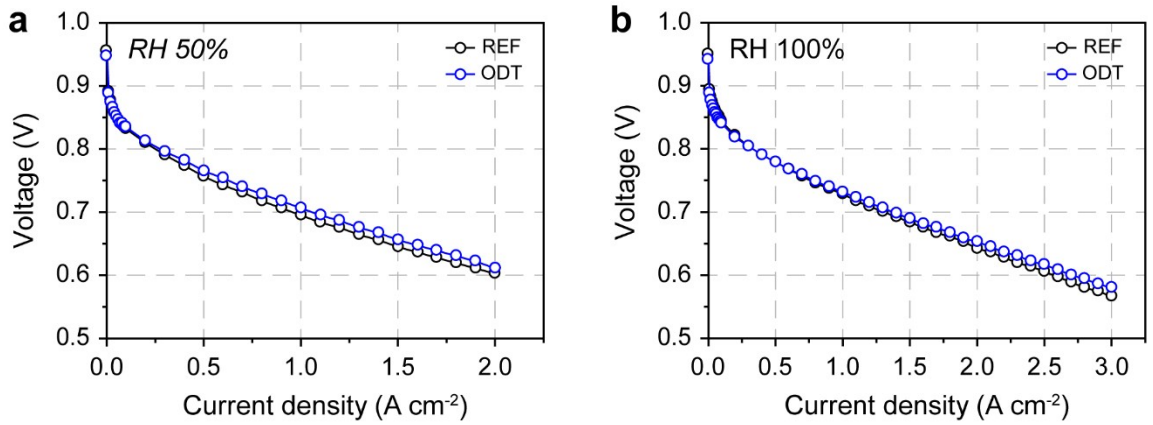

Fig. S11 Comparison of the IV polarization curves under H_2/O_2. (a, b) IV polarization curves at RH 50% (a) and at RH 100% (b).

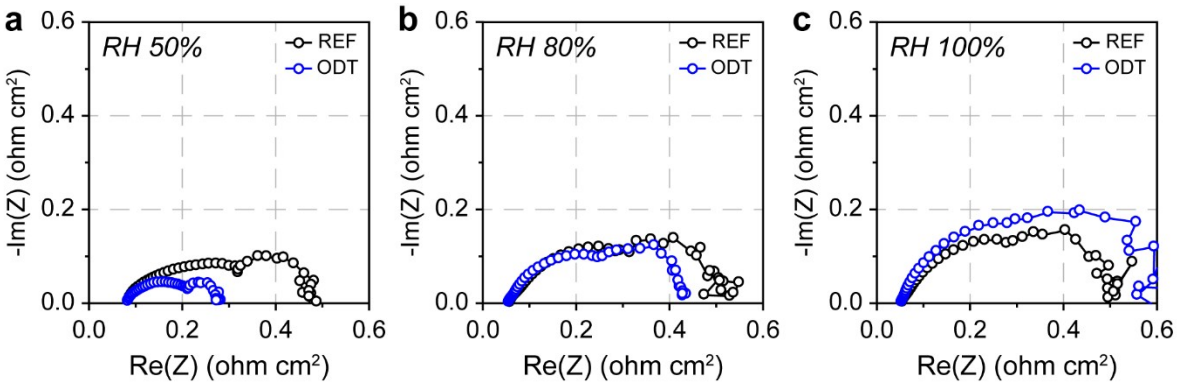

Fig. S12 Impedance analysis at different RHs. (a-c) Nyquist plots of the complex impedances at 1.5 A cm^{-2} at RH 50% (a), RH 80% (b) and RH 100% (c). The first circles represent the kinetic resistances for the ORR and the second stand for the mass transport resistance in the cathode CLs.